Supporting Information for:

S_0-State Model of the Oxygen-Evolving Complex of Photosystem II

Rhitankar Pal[1], Christian F. A. Negre[1], Leslie Vogt[1], Ravi Pokhrel[1], Mehmed Z. Ertem[1,2], Gary W. Brudvig[1*], and Victor S. Batista[1*]

[1]Department of Chemistry, Yale University, New Haven, CT 06511, United States.

[2] Department of Chemistry, Brookhaven National Laboratory, Building 555A, Upton, New York 11973, United States.

Section I. Description of Computational Methods.

Section II. Preliminary Monte Carlo results.

Section III. S_1 state of the OEC: EXAFS spectra of the QM/MM and comparison with the DFT small models.

Section IV. QM/MM and R-QM/MM geometry comparison between the O4H and O5H models of the S_0 state.

Section V. Distance comparison in the two S_0 models.

Section VI. Energetics of the proton-transfer pathway in S_0 state.

Section VII. XYZ coordinates of the QM layer of the S_0 state.

Section VIII. Extended Acknowledgement.

Section I. Description of Computational Methods.

QM/MM Model Selection

To construct a computational model of the OEC of PSII, coordinates were taken from the 1.9 Å crystal structure (PDB: 3ARC)[1] (see Figure S1). The model includes residues with C_α atoms within 15 Å of the atoms in the $CaMn_4O_5$ cluster and the two chloride ions near the OEC. Oxygen atoms of water molecules that fall within the 15 Å boundary were also included (85 total). Where the selection caused a gap of up to two residues in a peptide chain, the missing residues were added to provide continuity. Neutral capping groups (ACE/NME) were added for each chain break, with positions determined by the backbone atoms of neighboring residues. A few residues on the periphery of the selection were removed because their side chains extended away from the rest of the selection.

The final protein selection includes the following residues (capping residues in parenthesis use only the backbone atoms):
D1 (chain A): (57)-58-67-(68), (81)-82-91-(92), (107)-108-112-(113), (155)-156-192-(193), (289)-290-298-(299), (323)-324-344:C-terminus
CP43 (chain C): (290)-291-(292), (305)-306-314-(315), (334)-335-337-(338), (341)-342-(343), (350)-351-358-(359), (398)-399-402-(403), (408)-409-413-(414)
D2 (chain D): (311)-312-321-(322), (347)-348-352:C-terminus

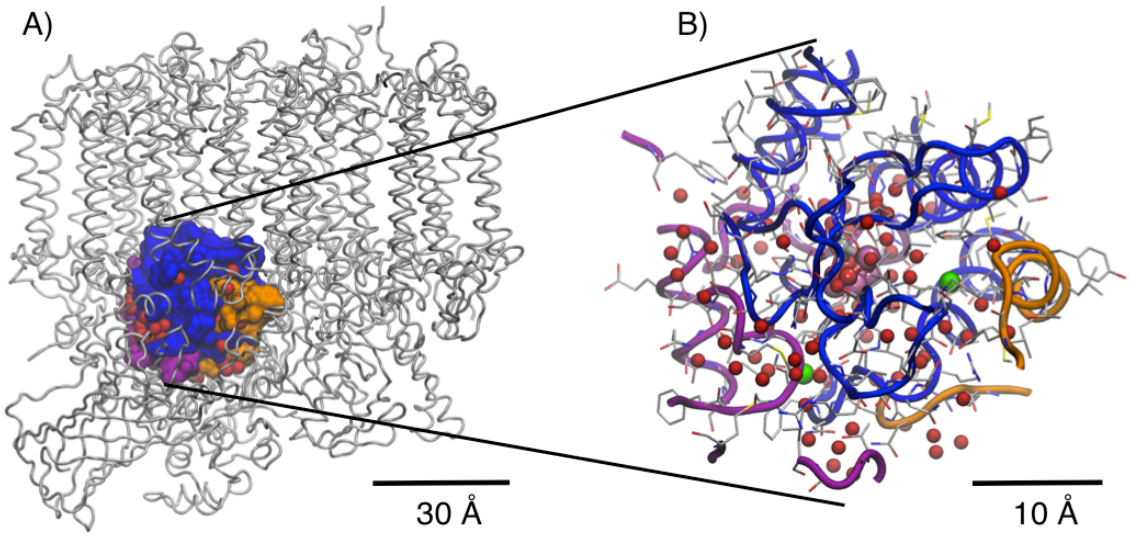

Figure S1. Atoms included in the QM/MM model belong to residues with C_α atoms within 15 Å of the OEC. A) Selected residues from monomer 1 of the 1.9 Å structure are shown with colored surfaces (chain A: blue, chain C: purple, chain D: orange, HOH O atoms, red) and the rest of the protein is indicated in grey. B) An expanded view of the selection with the OEC (shiny spheres with Mn (pink), Ca (grey), O (red)) visible in the center of the model. Two chloride ions (green spheres) are also included in the model.

Hydrogen atom placements were guessed using the AmberTools12 software package.[2] All acidic residues (ASP, GLU) were modeled as anions. Histidine protonation patterns

were determined by inspection: His190 is protonated at N_δ to be a hydrogen-bond acceptor from D1-Tyr161, His332 is protonated at N_δ to leave N_ε as a ligand to Mn2, and His337 is protonated so that N_ε donates a hydrogen bond to O3. Sodium counter ions were added based on the electrostatic potential outside the protein to neutralize the system. Hydrogen atom placements were refined by 500 steps of minimization using NAMD v.2.8[3] using molecular mechanics force field parameters, with all heavy atoms fixed in their x-ray assigned positions. Charges on the OEC atoms were assigned as previously reported.[4]

QM/MM Structure Optimization

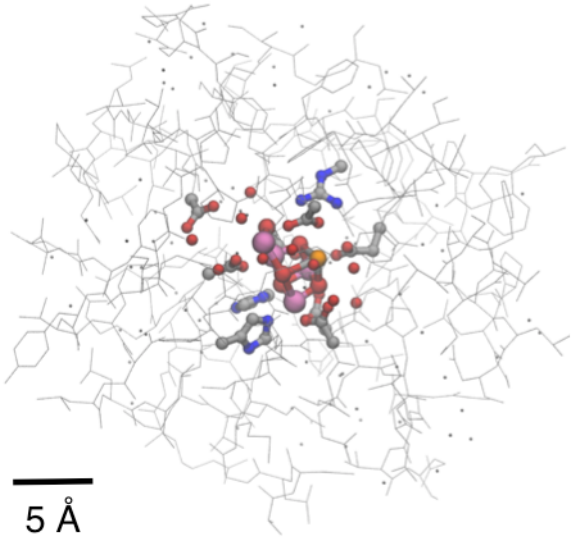

Figure S2. Heavy atoms described using DFT in the QM/MM model are shown in CPK representation (C: grey, N: blue, O: red, Mn: pink, Ca: orange, hydrogens omitted for clarity) with the Molecular Mechanics layer shown in grey lines.

The QM/MM optimizations for the S_0 and S_1 states were performed using the ONIOM method[5] as implemented in Gaussian09 software package.[6] The QM layer was modeled at the B3LYP[7, 8] level of theory using the LaNL2DZ[9, 10] basis set for Mn, Ca and 6-31G*[11] basis set for C, H, N and O. The QM region was chosen to include the OEC, all directly ligated side chains (D1-D170, D1-E189, D1-H332, D1-E333, D1-D342, and CP43-E354), the C-terminus of D1-A344, hydrogen-bonded residues D1-H337 and CP43-R357, residue D1-D61, and ten water molecules, as shown in Figure S2. The anionic ligands were modeled as acetate, D1 C-terminus as propanoate, histidines as methylimidazoles, and arginine as methylguanidinium in the QM layer. The AMBER force field[2] was used to model the MM region (Figure S2). All the atoms were allowed to relax during the QM/MM optimizations with the exception of the chloride ion, neutral capping groups (ACE/NME) and oxygen atoms of water molecules in the MM region.

Simulated Annealing Monte Carlo (MC) method

The simulation was performed by harmonically constraining all the surrounding ligands and relaxing the metal oxide core of the OEC. This is done in order to restrict the mobilities to the atoms within the cluster, which are known to be responsible for affecting the experimental EXAFS of the S-state intermediates during the photocycle. Each MC step consists of an attempt to move all the movable atoms (10/11 atoms for the cage) according to the Metropolis algorithm.[12] The probability of accepting the new position is given by:

$$P = \min\{1, e^{[-\Delta F/k_B T]}\} \qquad \ldots (1)$$

In equation (1), k_B is the Boltzmann constant, T is the temperature (which in this case is varied exponentially from an initial value to 0 K), and ΔF denotes the total cost function difference of the system between the final and the initial state. The cost function is calculated by taking the sum of the square deviations between the experimental EXAFS spectra with respect to the calculated one. In order to harmonically constrain the atoms, an additional penalty of $k.||\boldsymbol{r}-\boldsymbol{r}_{int}||^2$ was added to the cost function, where $\boldsymbol{r}-\boldsymbol{r}_{int}$ is the displacement vector with respect to the initial position $\boldsymbol{r}_{int}$. In this work, we employed the values of $k=100$ to harmonically constraint the atoms. We have performed 10 annealings with 20 temperature steps with the temperature being varied from 100 to 0 K with a decaying constant of 0.2 K/T step.

Calculation of the EXAFS

FEFF 8.30[13] combined with IFEFFIT[14] v.1.2.11d programs were used to compute the EXAFS spectra of the S_1 and S_0 models. Only the QM layers were taken into account for computing the EXAFS of the QM/MM optimized structures. For the current calculations, we considered all paths with lengths up to eight scattering legs and the extremely small contribution from hydrogen atoms was not considered. A value of 0.003 Å for the Debye–Waller factors was employed in all calculations. The energy (E) axis was converted into photoelectron wave vector (k) space by using the following transformation; $k = \frac{\sqrt{2m_e(E-E_0)}}{\hbar}$ where m_e is the mass of the electron and $\hbar = h/2\pi$ where h is Planck's constant. A value of E_0 = 6540.0 eV for the Fermi energy has been employed for the calculations involving the QM/MM model. A fractional cosine-square (Hanning) window with Δk = 1 was applied to the k^3-weighted EXAFS data. The grid of k points, which are equally spaced at 0.05 $Å^{-1}$ was then used for the Fourier transformation (FT) to R space. A k range of 2.29 – 11.5 $Å^{-1}$ for the FT for the isotropic EXAFS data was employed. The FT magnitude and EXAFS χk^3 values were appropriately scaled to match the experimental data.

Section II. S_1 state of the OEC: EXAFS spectra of the QM/MM and comparison with the DFT small models.

The overall calculated spectrum of the QM/MM model was in excellent agreement with the experimental spectrum. However, the peaks in the 4.0-5.0 $Å^{-1}$ and 8.0-9.0 $Å^{-1}$ regions were slightly shifted for the QM/MM model as compared to the experimental spectrum. MC refinements showed minor movements (RMSD = 0.04 Å) for the OEC atoms and corrected the location of previously offset peaks. The intermetallic bond lengths for the QM/MM and R-QM/MM structures are listed in Table 1. The extremely small changes in bond lengths (<0.1 Å) are indicative of the reliability of the QM/MM model for predicting the S_1 state structure.

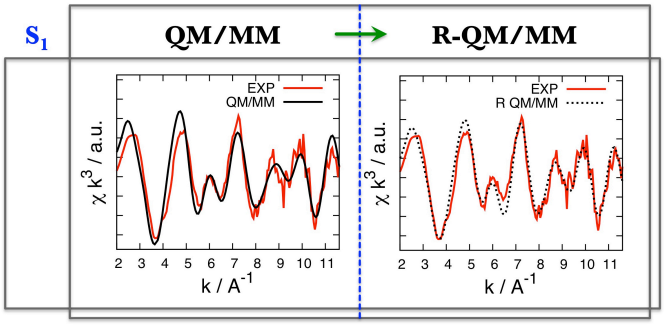

Figure S3. The experimental and calculated EXAFS χ-space spectrum ($\chi.k^3$ vs. k) of the QM/MM optimized and Monte Carlo refined (R-QM/MM) S_1 state model.

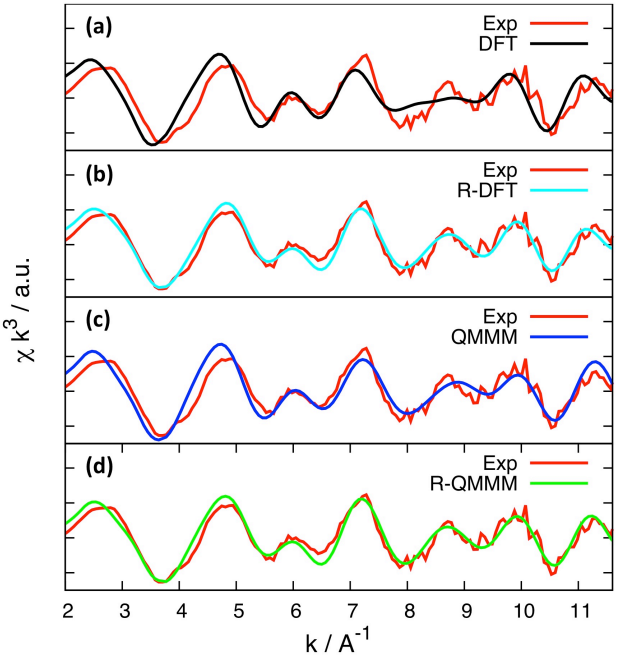

Figure S4. EXAFS spectra of S_1 DFT, R-DFT, QM/MM and R-QM/MM models are plotted against the experimental spectrum.

The small cluster model with only the QM layer atoms (as described in the manuscript) for the S_1 state was obtained starting from the X-ray crystal structure orientation and optimizing at the B3LYP/LACVP* level of theory. Subsequent MC refinement (R-DFT) was performed using a simulated annealing technique. The EXAFS of the cluster models (DFT and R-DFT) is plotted and compared in Figure S4. The EXAFS for the DFT cluster model [Figure S4(a)] clearly shows a poor match with the experimental spectra in the region 7-11 $Å^{-1}$ when compared to the EXAFS of QM/MM model [Figure S4(c)]. This observation suggests that the effect of adding the protein environment using the QM/MM model helps to fix the EXAFS spectrum.

Section III. Preliminary Monte Carlo results.

To determine the likely site for protonation of the OEC in the S_0 state, a preliminary MC screening using a simulated annealing algorithm[12] to fit the S_0 EXAFS data was performed on the geometry of the S_1 model. The model was composed of the metal oxide cluster, the functional groups of the residues which are directly coordinated and the hydrogen-bonded water network around the OEC. An overlay of the OEC geometry for the MC-prescreened S_0 state and the S_1 state is shown in Figure S5a. MC optimization revealed that the Mn3, Mn4, O4, and O5 atoms of the OEC had significant movements, thereby suggesting possible protonation at the O5/O4 μ-oxo bridge in the S_0 state. Furthermore, this also indicates that either Mn3 or Mn4 is oxidized during this transition to induce the requisite geometry change. This result is in agreement with the reported B-factors of the atoms in X-ray crystal structure at 1.9 Å resolution (PDB: 3ARC).[1] The O4 and O5 atoms exhibit the highest displacement among all the bridging μ-oxos (see Figure S5a). This is reasonable because the X-ray structure most likely had significant radiation damage and, therefore, the reported X-ray structure of the OEC has been suggested to represent the S_{-3} state[15, 16] or a mixture of different reduced S states [17, 18]. In addition, protonation at O4 or O5 is reported to be energetically more favorable than O1 in model clusters in reduced states.[16] The other μ-oxo sites are unlikely to be protonated, as O2 is near the positively charged R357 and O3 is strongly hydrogen bonded to H337. In light of these observations, we explored the protonation of O4 and O5 sites using the QM/MM model of the S_0 state.

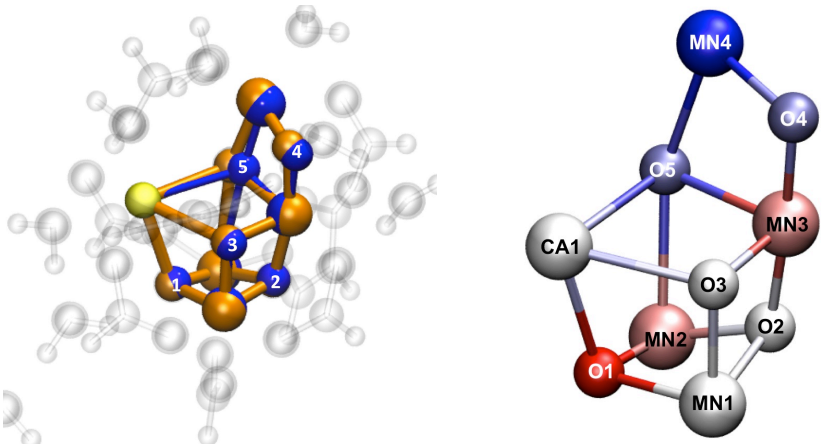

(a) (b)

Figure S5. (a) A geometric overlay of the preliminary Monte Carlo (MC) refined $CaMn_4O_5$ cluster of the S_0 state (in orange) and the actual S_1 state (in blue) structures. The MC refinements were performed starting from the S_1 state geometry and cost functions were evaluated based on the S_0 state experimental EXAFS to ensure the geometry relaxation occurs towards S_0 state. (b) The color-coded beta-factors (values taken from the 3ARC X-ray crystal structure) on the atoms of $CaMn_4O_5$ cluster of the OEC. The most uncertain positions are represented by blue colors and the least uncertain is red. The white colored atoms are of medium uncertainty. The position of dangling Mn atom (Mn4) along with the O4 and O5 atoms are the most uncertain.

Section IV. QM/MM and R-QM/MM geometry comparison between the O4H and O5H models of the S_0 state.

The S_0 state models were obtained by optimizing either the O5- or O4-protonated X-ray structure with the same QM/MM method used for the S_1 state. Subsequent refinement of the QM/MM structures was performed with the simulated annealing MC method as described in Section III.

The EXAFS spectra of the O4-H and O5-H models (QM/MM and R-QM/MM) are shown in Figure 2. It is evident that the 8-11.6 $Å^{-1}$ region of the experimental EXAFS matches better with the O5-H QM/MM model than with O4-H. While the R-QM/MM models for both O5-H and O4-H fit well, RMSD of the $CaMn_4O_5$ cluster for O5-H is much lower (0.05 Å) than the RMSD for O4-H (0.12 Å), indicating that smaller refinements are needed for proper fitting of the O5-H EXAFS to experimental data. An overlay of the QM/MM and R-QM/MM structures of the S_0 state of the OEC in which either O5 or the O4 is protonated are shown in Figure S6 below. The O5-H structure clearly shows minimal movements, whereas O4-H undergoes more significant structural changes during the MC refinement. This reinforces the fact that QM/MM O5-H structure is most likely closer to the actual S_0 state structure observed by EXAFS measurements.

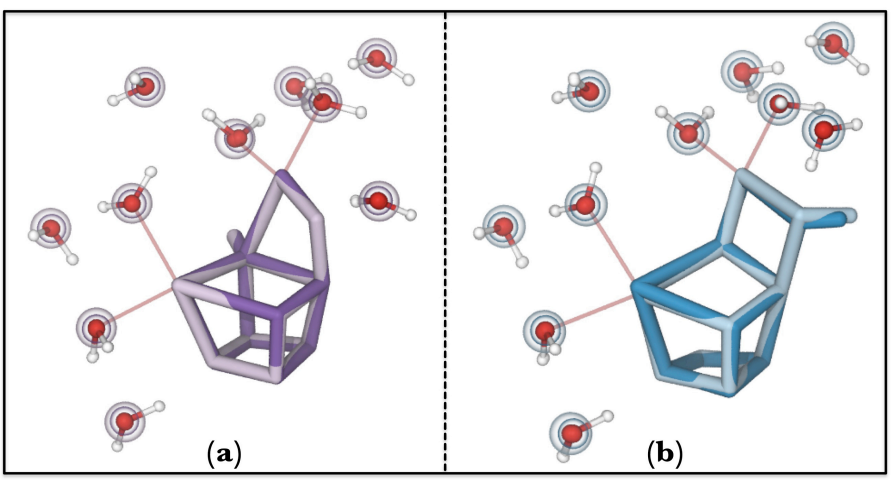

Figure S6. An overlay of the QM/MM (darker color) and R-QM/MM (lighter color) structures for (a) O5-H and (b) O4-H models for the S_0 state of the OEC. For the water molecules, the two concentric circles are centered on the QM/MM (inner) and R-QM/MM (outer) positions for the O atoms.

Section V. Distance comparison in the two S_0 models.

The intermetallic (Mn-Mn and Mn-Ca) distances for the two S_0 state models in Table S1 and the Mn-O distances are summarized in Table S2.

Table S1.

S_0	O5 -H QM/MM	MC-refined R-QM/MM	O4-H QM/MM	MC-refined R-QM/MM
Mn1--Mn2	2.72	2.74	2.71	2.77
Mn1--Mn3	3.20	3.19	3.50	3.51
Mn1--Mn4	4.72	4.66	5.07	5.09
Mn2--Mn3	2.77	2.76	2.83	2.77
Mn2--Mn4	5.25	5.19	5.28	5.25
Mn3--Mn4	2.95	2.90	2.89	2.94
Ca^{2+}--Mn1	3.37	3.41	3.58	3.36
Ca^{2+}--Mn2	3.46	3.45	3.39	3.18
Ca^{2+}--Mn3	3.72	3.73	3.53	3.44
Ca^{2+}--Mn4	3.92	3.91	3.79	3.83

Table S2.

S_0	O5 -H QM/MM	MC-refined R-QM/MM	O4-H QM/MM	MC-refined R-QM/MM
Mn1-O1	1.86	1.92	1.85	1.84
Mn1-O3	1.89	1.84	1.83	1.77
Mn1-O5	2.35	2.31	3.35	3.30
Mn2-O1	1.85	1.88	1.85	1.98
Mn2-O2	1.79	1.76	1.77	1.72
Mn2-O3	1.84	1.86	1.85	1.86
Mn3-O2	1.86	1.80	1.85	1.90
Mn3-O3	2.00	1.99	2.25	2.32
Mn3-O4	1.85	1.87	2.14	2.35
Mn3-O5	2.43	2.41	1.90	1.85
Mn4-O4	1.75	1.78	2.30	2.36
Mn4-O5	2.49	2.45	1.79	1.86
Ca^{2+}-O1	2.41	2.34	2.44	2.29
Ca^{2+}-O2	2.76	2.80	2.62	2.46
Ca^{2+}-O5	2.41	2.51	2.51	2.45

Section VI. Energetics of the proton-transfer pathway in S_0 state.

The favorable proton-transfer pathway from the O5 atom to the hydroxo ligand on Mn4 atom of the OEC cluster in the (III, IV, IV, III) charge state is depicted in Table S3. The oxidation of the $CaMn_4O_5$ cluster, mediated by the redox-active $Y_Z^{\bullet}$ radical, is known to be the first event during the S_0 to S_1 PCET step. This is followed by a deprotonation in order to balance the accumulated charge during oxidation. We propose that, if the deprotonation occurs from the Mn4 bound w2 molecule (which is also connected to the D1-D61 via a hydrogen-bonding network as shown in Figure S7), then the O5 proton is spontaneously delivered to w2-hydroxo group.

Table S3.

H---O5 distance (Å)	**1.1**	**1.3**	**1.5**	**1.7**	**1.9**	**2.1**	**2.3**
E (kcal/mol)	0.0	-0.8	-7.4	-11.5	-13.8	-15.2	-17.3

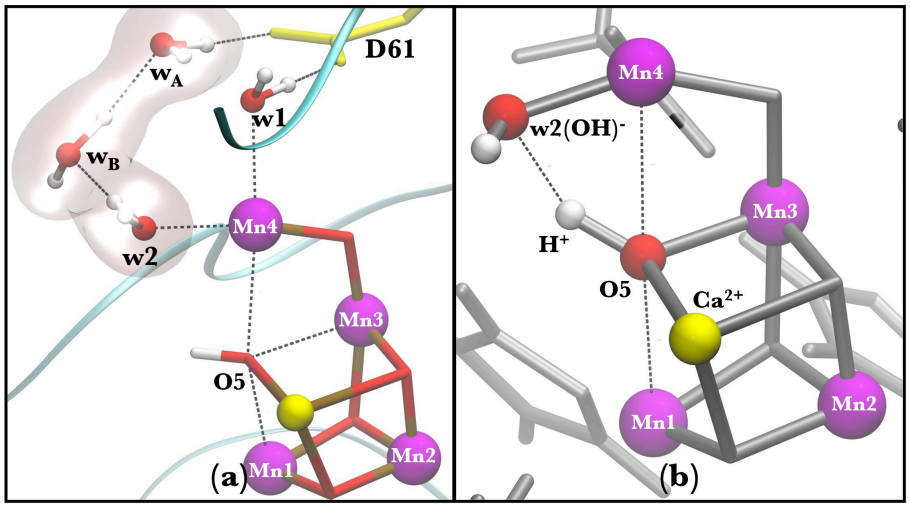

Figure S7. (a) Hydrogen-bond network, from Mn4(w2) to D1-D61, in the QM/MM S_0 state model where O5 is protonated. Dashed lines indicate hydrogen bonds and other non-covalent interactions. The D61 residue is highlighted in yellow and the water molecules forming a hydrogen-bond network essential for a Grotthuss-like proton-transport mechanism are shown surrounded by a glossy surface. (b) A small model of the oxidized S_0' state, with Mn3(IV) and a deprotonated w2 as a hydroxyl ion. The O5-H is found to be hydrogen bonded to the w2 hydroxyl group.

Section VII. XYZ coordinates of the QM layer of the S_1 and S_0 state.

S1
1. QM/MM optimized

O	-26.341590	-36.539379	204.075251
Ca	-27.638861	-36.734153	202.017497
Mn	-24.859489	-35.460109	203.824731
O	-28.300663	-34.764075	203.814905
Mn	-27.250339	-35.321113	205.133412
O	-25.979850	-34.128194	204.505113
Mn	-27.279398	-33.368785	203.187466
O	-28.507397	-32.828509	202.019617
Mn	-27.562990	-33.369417	200.518448
O	-26.639656	-34.366692	201.815633
C	-28.484382	-27.474049	201.611608
H	-28.001475	-26.494651	201.600704
H	-28.352400	-27.933099	202.597396
C	-27.842378	-28.411308	200.580635
O	-28.465856	-29.453950	200.243506
O	-26.711201	-28.078221	200.100014
C	-30.782423	-36.129176	198.951248
H	-31.816231	-36.183213	199.308195
H	-30.508487	-37.155316	198.666151
C	-29.843649	-35.753475	200.100745
O	-29.976511	-36.367105	201.201981
O	-28.943698	-34.895568	199.879625
C	-23.167313	-38.990696	202.698771
H	-23.077620	-39.048490	203.789115
H	-22.202252	-38.636253	202.318954
C	-24.170919	-37.899733	202.397845
O	-25.221431	-38.053101	201.743410
O	-23.798687	-36.785059	202.923686
C	-20.439941	-32.782810	201.643727
H	-20.918620	-32.693671	200.665483
H	-19.611545	-33.494396	201.550361
C	-21.448693	-33.339675	202.584980
N	-21.189472	-33.641912	203.909829
H	-20.318846	-33.495694	204.428801
C	-22.289599	-34.178546	204.457206
H	-22.355962	-34.541155	205.466928
N	-23.263625	-34.237029	203.556353
C	-22.752515	-33.715237	202.382451
H	-23.351426	-33.648327	201.486356
C	-24.658500	-30.293544	201.635172
H	-25.144035	-29.398470	201.230229

H	-23.915085	-30.624878	200.905573
C	-25.697936	-31.390506	201.709177
O	-26.071383	-31.838754	202.849405
O	-26.136753	-31.793349	200.597311
C	-24.226347	-31.026926	209.744811
H	-23.226538	-30.639200	209.966072
H	-24.458338	-31.796251	210.491785
C	-24.208655	-31.585382	208.358095
N	-23.373472	-31.019032	207.420017
C	-23.644264	-31.605726	206.276887
H	-23.148315	-31.395299	205.344162
N	-24.626382	-32.533075	206.423160
H	-25.058895	-33.080446	205.679717
C	-25.002742	-32.531418	207.753934
H	-25.763295	-33.194517	208.134791
C	-24.331118	-36.790918	208.004309
H	-23.594413	-36.063167	208.363328
H	-23.767426	-37.702663	207.795366
C	-24.916287	-36.235556	206.730656
O	-26.143662	-35.912509	206.727355
O	-24.115012	-36.083723	205.753600
C	-29.826653	-38.492791	206.056347
H	-29.680913	-39.490858	205.624308
C	-31.317366	-38.154247	206.145854
H	-31.460793	-37.116970	206.461324
H	-31.785063	-38.283778	205.167259
H	-31.847375	-38.812888	206.847775
C	-29.111757	-37.488660	205.161412
O	-29.136375	-37.625281	203.926548
O	-28.549605	-36.538309	205.820679
C	-28.604411	-31.745214	207.061937
H	-28.803005	-30.777853	206.600327
H	-27.807598	-31.602866	207.801438
C	-28.132079	-32.715346	205.995109
O	-27.926608	-33.924153	206.366877
O	-27.965635	-32.266663	204.822380
C	-34.156263	-34.978473	204.746661
H	-33.710635	-35.762326	205.364537
H	-34.746674	-35.474605	203.966812
N	-33.119884	-34.125764	204.198752
H	-33.333327	-33.140842	204.055175
C	-32.019901	-34.557993	203.546427
N	-31.713866	-35.857668	203.495440
H	-32.432770	-36.550984	203.695770
H	-30.980777	-36.151841	202.844357
N	-31.221373	-33.655261	202.971674

H	-31.481783	-32.674965	203.007074
H	-30.260173	-33.872552	202.702826
O	-26.276238	-39.305660	204.687801
H	-25.477019	-39.624631	205.166645
H	-26.202028	-38.324371	204.618656
O	-27.731916	-39.230439	202.319039
H	-26.950690	-39.479305	202.854557
H	-28.469221	-39.238471	202.959676
O	-27.284854	-37.193949	199.662538
H	-26.581135	-37.828767	199.407372
H	-27.377998	-36.585315	198.904402
O	-27.242638	-35.992492	197.082555
H	-26.584838	-36.723868	196.905270
H	-28.090289	-36.328402	196.715304
O	-26.408200	-33.942888	198.883601
H	-26.842079	-34.458705	198.173913
H	-25.847922	-33.224003	198.471223
O	-28.602755	-32.009186	199.355367
H	-28.161941	-31.136738	199.536370
H	-29.471074	-31.865589	199.819011
O	-24.846217	-32.023040	197.735924
H	-24.060928	-31.966428	198.311235
H	-25.342860	-31.189270	197.956809
O	-26.107112	-29.598970	198.053985
H	-26.358203	-29.141267	198.928768
H	-26.965006	-29.751105	197.630804
O	-30.375963	-31.089320	201.157864
H	-29.774686	-31.557714	201.780943
H	-29.864386	-30.260868	200.973857
O	-25.316342	-39.181513	199.226427
H	-26.123448	-39.739166	199.319134
H	-25.109632	-38.924854	200.157539

2. MC refined (R-QM/MM) model:

O	-26.2891574110637	-36.5235607013275	204.173827056776
Ca	-27.6036439552357	-36.7866395545298	201.990116517015
Mn	-24.8866157802307	-35.4431280738403	203.774157004018
O	-28.3707135461215	-34.7122179854371	203.864574889103
Mn	-27.2572766407987	-35.3123696445247	205.140454149311
O	-25.9568704118438	-34.1581143705942	204.486457562380
Mn	-27.3371094405514	-33.3562529994728	203.202617464517
O	-28.3950522090285	-32.9102771087764	202.113056863560
Mn	-27.5671485152155	-33.3984632855090	200.506433022404
O	-26.7140707318882	-34.3542359727289	201.796663242582
C	-28.4945946729526	-27.4347620429058	201.610464895418

H	-28.0325241616191	-26.4998909786270	201.627273367523
H	-28.3533509324953	-27.8855720998881	202.583088939712
C	-27.8272478127367	-28.4063183237109	200.588458234013
O	-28.4634783882496	-29.4370342422305	200.212963255202
O	-26.7179570497843	-28.0768314684274	200.089566486053
C	-30.8121184686677	-36.1272520079149	198.959375178514
H	-31.8126936504251	-36.1480426543708	199.316842061211
H	-30.4757563197495	-37.1532969745492	198.644896885246
C	-29.8582340184762	-35.7805554805544	200.086429367101
O	-29.9543372483493	-36.3466200063915	201.193905061499
O	-29.0078726257134	-34.9473268154149	199.852276551195
C	-23.1681220322954	-39.0113473766195	202.702363841519
H	-23.0527803235118	-39.0680865453910	203.785151076275
H	-22.1980484458935	-38.6365994324537	202.357138387735
C	-24.1402104932104	-37.9374744884141	202.354783469137
O	-25.2359644858874	-38.0301877772033	201.773593049028
O	-23.7957860425370	-36.7101718839752	202.952016557276
C	-20.4341871009246	-32.7875049897714	201.669083361243
H	-20.9571153824164	-32.6999164923796	200.655328545876
H	-19.6407135381619	-33.5176716601008	201.518915231285
C	-21.4544233901192	-33.3212881726211	202.579799642615
N	-21.1537719918330	-33.6197250774161	203.907964813479
H	-20.3029213720082	-33.4881660256826	204.431851193714
C	-22.3100970622927	-34.2389283053001	204.567572099964
H	-22.3201118924726	-34.5377760007683	205.490127596358
N	-23.3372889275720	-34.1819869658509	203.581928473815
C	-22.8150426893563	-33.7536317133383	202.393935528147
H	-23.3477734604034	-33.5928976898162	201.480863503454
C	-24.6945763572757	-30.2746357546648	201.630452395663
H	-25.1412643595473	-29.3658552237624	201.256990696490
H	-23.9149835117756	-30.6246339813308	200.933657552268
C	-25.6557849347325	-31.3563348566258	201.737670926323
O	-26.0388047988269	-31.8417110267746	202.848704889347
O	-26.0126149063671	-31.6440857182494	200.586647327644
C	-24.2460701964681	-31.0092787095723	209.744651969900
H	-23.2702937383938	-30.6085334066453	209.928289697525
H	-24.4663039568127	-31.7994610877802	210.487992069033
C	-24.2214644842547	-31.5920740741025	208.352763710446
N	-23.3284738901457	-31.0444456416832	207.406452200123
C	-23.6627402697340	-31.6347581496529	206.262875313780
H	-23.1401352231005	-31.4161322855541	205.361765319429
N	-24.6087931478135	-32.5856205255196	206.358485702229
H	-25.0469017886330	-33.0865710391934	205.641480398971
C	-24.9912109389020	-32.5238597485067	207.783534844468
H	-25.7708806407280	-33.1907769604031	208.107096604032
C	-24.3335103878763	-36.7616162865609	207.991856876037

H	-23.5599426192016	-36.0315765433866	208.389347088242
H	-23.7721971424861	-37.7151901274413	207.799513757683
C	-24.9316240330360	-36.2117068828718	206.721511767047
O	-26.1186682203852	-35.8970106866143	206.692572867578
O	-24.0595131390700	-36.1586513550570	205.880362453373
C	-29.8170110374401	-38.4962578122393	206.057228229265
H	-29.6834312792284	-39.4810680720060	205.662237108116
C	-31.2938994302322	-38.1073433269328	206.143066694315
H	-31.4817164579657	-37.1008290139363	206.493638512522
H	-31.7804468656285	-38.2694018722000	205.184348524930
H	-31.8249122503340	-38.8193161663433	206.867471675677
C	-29.1126419002218	-37.5075038523016	205.188053156528
O	-29.1157881772593	-37.6248636156528	203.923981106558
O	-28.5502255234049	-36.4887508286495	205.792510838492
C	-28.6146086847762	-31.7526265775218	207.042036491738
H	-28.8022045407592	-30.7993866459306	206.572436529919
H	-27.7996413849672	-31.5920394315570	207.766357965501
C	-28.1480377496980	-32.7116504992175	206.020784250320
O	-27.9543637724257	-33.8764500850499	206.331112574146
O	-27.9615642260425	-32.2917375339174	204.835995748738
C	-34.1314099268114	-35.0117644873689	204.766573136267
H	-33.6991763227491	-35.7624146985369	205.390470638008
H	-34.7549485286739	-35.4845126295613	204.005455755853
N	-33.1552445099456	-34.1359758674691	204.175016992040
H	-33.3480710433110	-33.1140282616764	204.018599762631
C	-32.0470106098053	-34.5848457847895	203.560447474784
N	-31.7073096334991	-35.8034057554355	203.508160467831
H	-32.4332951362284	-36.5296529031546	203.693771889488
H	-30.9567036208875	-36.1563763026295	202.878728710881
N	-31.2316807004232	-33.6413425351355	202.929822733200
H	-31.4542431508597	-32.7167120170498	203.039540833854
H	-30.2737494244933	-33.8983006574619	202.705873457909
O	-26.2336724125376	-39.3113704970959	204.758048674336
H	-25.4743136890898	-39.6410336206973	205.208937410127
H	-26.2096887245375	-38.3110991954255	204.641756905569
O	-27.6916615235156	-39.2162826358786	202.306460391366
H	-26.9334836299494	-39.4487118600713	202.862568374189
H	-28.4489209148498	-39.2301509568945	202.948445908952
O	-27.2853131554905	-37.1437572667193	199.691733782379
H	-26.6188728650366	-37.8002328812414	199.399040480174
H	-27.3639309692894	-36.5967537512398	198.894008233743
O	-27.2720099296299	-35.9956047091012	197.086024354247
H	-26.5653034825634	-36.7427358620663	196.927200104160
H	-28.0916199666861	-36.3196209080368	196.712125763220
O	-26.4149122613205	-33.9357644519518	198.900689881931
H	-26.8702115393810	-34.4483204597046	198.202349965192

H	-25.8684535549777	-33.1952848209240	198.471408148873
O	-28.5360506272492	-32.0033739154502	199.366504981566
H	-28.1177364899030	-31.1442452007984	199.577987333642
H	-29.4720923825095	-31.8778027890841	199.791578430892
O	-24.8502912852068	-31.9850120709534	197.811024003798
H	-24.0987206888439	-31.9395332175608	198.323972232389
H	-25.3422098732661	-31.1965840036183	197.959568716850
O	-26.1006591818324	-29.5909204769569	198.091612807305
H	-26.3311222201199	-29.1387793283967	198.923071840716
H	-26.9315061989660	-29.7457808301495	197.680177043026
O	-30.4008604835692	-31.1000611500360	201.142624031106
H	-29.7409022843714	-31.5876183352430	201.776727766283
H	-29.8818023006562	-30.2530438881060	200.953432418647
O	-25.3107884033993	-39.2092498354399	199.218904282184
H	-26.1474177791039	-39.7437467865675	199.327452285046
H	-25.0997276641237	-38.9352988591491	200.146646622399

S0

1. QM/MM optimized O5H model:

O	-26.339545	-36.522716	204.117472
Ca	-27.480343	-36.756814	202.012976
Mn	-24.908207	-35.408462	203.721577
O	-28.226130	-34.722719	203.729114
Mn	-27.241935	-35.262323	205.120825
O	-25.969470	-34.072621	204.534608
Mn	-27.222179	-33.249166	203.217260
O	-28.230356	-32.894652	201.710865
Mn	-27.290938	-33.246175	200.271551
O	-26.041212	-34.796739	201.758930
C	-28.477208	-27.480895	201.655900
H	-27.994781	-26.501408	201.611366
H	-28.352799	-27.897872	202.660734
C	-27.834906	-28.467286	200.664689
O	-28.454550	-29.536055	200.439373
O	-26.722465	-28.123221	200.136535
C	-30.374476	-35.940584	198.834503
H	-31.380439	-36.074148	199.244188
H	-29.989198	-36.942973	198.606541
C	-29.437873	-35.394563	199.909434
O	-29.535950	-35.856413	201.062430
O	-28.552062	-34.549699	199.512684
C	-23.139501	-39.007210	202.729483
H	-23.048171	-39.067052	203.819388
H	-22.174229	-38.655331	202.347446

C	-24.143991	-37.917640	202.426940
O	-25.191265	-38.089330	201.761678
O	-23.788463	-36.803387	202.951396
C	-20.412139	-32.736308	201.655516
H	-20.874621	-32.650296	200.669241
H	-19.576359	-33.440087	201.573245
C	-21.431558	-33.303570	202.576749
N	-21.199269	-33.626954	203.900972
H	-20.336980	-33.497570	204.438350
C	-22.317349	-34.159857	204.419528
H	-22.409212	-34.530657	205.424800
N	-23.274997	-34.197873	203.500371
C	-22.734656	-33.663037	202.346842
H	-23.312202	-33.557262	201.440786
C	-24.635032	-30.224317	201.619683
H	-25.179009	-29.364071	201.208324
H	-23.883449	-30.523915	200.887696
C	-25.601666	-31.369322	201.746917
O	-26.049479	-31.709457	202.877094
O	-25.902071	-31.948038	200.645857
C	-24.392049	-30.795318	209.777403
H	-23.402812	-30.388553	210.013212
H	-24.659442	-31.517887	210.561068
C	-24.319862	-31.463590	208.433493
N	-23.473489	-30.950315	207.474247
C	-23.713650	-31.611630	206.365476
H	-23.214686	-31.449438	205.422714
N	-24.680420	-32.546479	206.555990
H	-25.094237	-33.138746	205.835427
C	-25.081995	-32.464046	207.874943
H	-25.835143	-33.121160	208.275549
C	-24.298728	-36.727522	207.976376
H	-23.547197	-36.003342	208.306629
H	-23.745909	-37.644579	207.758445
C	-24.906241	-36.176066	206.705976
O	-26.138807	-35.860264	206.723501
O	-24.115625	-36.021155	205.726088
C	-29.743136	-38.518837	206.066034
H	-29.521439	-39.505440	205.638436
C	-31.259621	-38.297381	206.148177
H	-31.487163	-37.267454	206.430885
H	-31.717310	-38.490754	205.173815
H	-31.744255	-38.971857	206.868082
C	-29.102344	-37.464768	205.168393
O	-29.199292	-37.565908	203.922399
O	-28.543113	-36.513587	205.811064

C	-28.615413	-31.786905	207.249922
H	-28.716126	-30.764173	206.880819
H	-27.854949	-31.793651	208.037663
C	-28.162373	-32.671853	206.102729
O	-27.964468	-33.913857	206.384164
O	-28.004959	-32.148893	204.971283
C	-34.193059	-34.930261	204.760742
H	-33.759462	-35.706920	205.393751
H	-34.799552	-35.435896	203.999540
N	-33.131685	-34.128741	204.184513
H	-33.319239	-33.160806	203.928891
C	-31.929048	-34.616386	203.815565
N	-31.671224	-35.929970	203.999327
H	-32.451310	-36.584993	203.972769
H	-30.796395	-36.302951	203.635025
N	-30.983646	-33.824751	203.339237
H	-31.090301	-32.828445	203.088890
H	-30.052860	-34.220668	203.177944
O	-26.299354	-39.273432	204.724181
H	-25.496230	-39.611095	205.183287
H	-26.204210	-38.291475	204.663041
O	-27.752761	-39.206877	202.361181
H	-26.991582	-39.473412	202.919814
H	-28.503186	-39.170369	202.987269
O	-27.196269	-37.130164	199.559545
H	-26.507679	-37.791212	199.313702
H	-27.090398	-36.385510	198.945066
O	-26.762651	-35.657953	196.759858
H	-26.268454	-36.530126	196.768131
H	-27.684698	-35.926316	196.579935
O	-25.962586	-33.829208	198.791503
H	-26.320575	-34.328046	198.026534
H	-25.349977	-33.094092	198.455932
O	-28.127374	-31.616314	198.905158
H	-28.279274	-30.806190	199.502191
H	-28.953751	-31.822903	198.413190
O	-24.432601	-31.868567	197.874750
H	-23.599706	-31.687518	198.361269
H	-24.995983	-31.068014	198.061213
O	-26.124466	-29.749574	198.116820
H	-26.352215	-29.203947	198.937890
H	-26.839009	-30.421893	198.110818
O	-30.465745	-31.400204	202.064035
H	-29.650864	-31.874570	201.772035
H	-30.082110	-30.722468	202.683553
O	-25.307147	-39.157027	199.236488

H	-26.108011	-39.723535	199.332814
H	-25.088784	-38.915157	200.171450
H	-25.316406	-34.790030	201.113198

2. MC-refined (R-QM/MM) model:

O	-26.3895244100287	-36.5668713168247	204.062508413371
Ca	-27.5207250506157	-36.7891724083295	202.024519927653
Mn	-24.9063529316646	-35.4068834703859	203.713288183379
O	-28.1893951117991	-34.6843096824056	203.739750597059
Mn	-27.2543048176997	-35.2714886637572	205.114873265289
O	-25.9423412341080	-34.1014922704166	204.503784017897
Mn	-27.2160821657620	-33.2686440003830	203.217405210186
O	-28.2883416492888	-32.8900755392034	201.733841927432
Mn	-27.2871674866934	-33.2831430512195	200.316577676905
O	-26.0260031034744	-34.7923405741574	201.785104867188
C	-28.4768552954116	-27.4880970845166	201.647961406499
H	-27.9949011907366	-26.5055506315826	201.604370766933
H	-28.3638078923327	-27.9105599825768	202.667834450118
C	-27.8407390737530	-28.4904266868194	200.669752364456
O	-28.4531833985156	-29.5591826550753	200.453856641766
O	-26.7151240751017	-28.1267320879304	200.136426568748
C	-30.3976062532995	-35.9393827808437	198.843480416993
H	-31.4182478682605	-36.0616984585992	199.243163126789
H	-29.9822632702655	-36.9466217991765	198.626199544923
C	-29.4601497990547	-35.3785801020118	199.944194159835
O	-29.5239449158195	-35.8650115848125	201.048056568984
O	-28.5644292335356	-34.4925721581111	199.501384198860
C	-23.1381893176146	-39.0096247698506	202.697740510483
H	-23.0890123574840	-39.0656202202227	203.832169824567
H	-22.1762788926457	-38.6582680146045	202.331809234338
C	-24.1656879207659	-37.8727921666932	202.445708290783
O	-25.1839310132602	-38.0500015984093	201.749457825524
O	-23.8460658324937	-36.8119271653607	202.946006875859
C	-20.4177993369215	-32.7078597570180	201.644629049663
H	-20.8886820108188	-32.6405535473694	200.639674235599
H	-19.6013169066772	-33.4518036223771	201.572744485177
C	-21.4118176981041	-33.2879702169203	202.591150181589
N	-21.1950210673378	-33.6484738425741	203.915994799155
H	-20.3654609003943	-33.5323061755133	204.417119513692
C	-22.2709294177189	-34.1246434965987	204.452378932722
H	-22.4304481957319	-34.5529085856923	205.436822100597
N	-23.2075404481364	-34.1667838554454	203.515474715165
C	-22.7472153682978	-33.7042842214840	202.316895756382

H	-23.3128220392307	-33.5643756727864	201.442270476691
C	-24.6155481094410	-30.2035438902601	201.632577242060
H	-25.2065736518825	-29.3570831975688	201.195735768358
H	-23.8801197456878	-30.5209078848822	200.908868060241
C	-25.5955216884486	-31.4207687630584	201.765655201019
O	-26.0402042810484	-31.7390236756635	202.825728904266
O	-25.9760126821732	-31.9023963610132	200.652548797872
C	-24.3894391392441	-30.7712534158791	209.789709304996
H	-23.4040986075893	-30.3413735599588	210.016379173939
H	-24.6536789107321	-31.4953360710852	210.544912246693
C	-24.2859207493225	-31.4961010191949	208.435397955646
N	-23.4991957035640	-30.9549808385471	207.479729643099
C	-23.7148084882152	-31.5983480146841	206.371966654965
H	-23.2308772700982	-31.4701714062142	205.444225167208
N	-24.6782635812247	-32.5285997284486	206.588858585651
H	-25.1117323141073	-33.1403664670131	205.823331325895
C	-25.1028107810822	-32.4914038576746	207.876446724723
H	-25.8592658863133	-33.1242846808663	208.290705413539
C	-24.3135152059056	-36.7321428797338	207.989721329095
H	-23.5465141101864	-36.0001015021820	208.314835464559
H	-23.7584320636631	-37.6553221751621	207.754308689819
C	-24.8482178021293	-36.2428757593956	206.706506937242
O	-26.1246565706388	-35.8268313318532	206.781071009798
O	-24.0345162885756	-36.0552522383499	205.752696867274
C	-29.7431360000000	-38.5188370000000	206.066034000000
H	-29.5288005519508	-39.4951462948963	205.667585882770
C	-31.2886997367717	-38.2672588469533	206.136097492107
H	-31.4653780838516	-37.2649034397329	206.450444145026
H	-31.7297622038600	-38.4634201131317	205.167657250965
H	-31.7427669239478	-38.9462517377131	206.875431618076
C	-29.0799124288381	-37.4406382774003	205.083146522301
O	-29.1550281089741	-37.4705016949216	204.011419859138
O	-28.5413215981512	-36.5434714381306	205.805341156349
C	-28.6018436034155	-31.7770883662021	207.243877977359
H	-28.7104187949083	-30.7502401199582	206.884412767495
H	-27.8995000499467	-31.8142169231511	208.050545629535
C	-28.1302698958539	-32.7109429224429	206.099094579691
O	-27.9580979799399	-33.9483335385406	206.397704156826
O	-28.0576478003706	-32.1794475787081	205.010350535252
C	-34.1920192191777	-34.9545027424617	204.768242350900
H	-33.7851504412880	-35.7123962724975	205.390327909574
H	-34.8108403432230	-35.4535604062281	204.014873582940
N	-33.1568583632536	-34.1566327923492	204.186309064719
H	-33.2789680172367	-33.1782960349167	203.878395945314
C	-31.9345215984200	-34.6277395044494	203.822662730281
N	-31.6667446844405	-35.9458618618286	204.042341556981

H	-32.4701266539822	-36.5783280913208	204.008369054457
H	-30.7993848083206	-36.2857257434312	203.638086274572
N	-30.9955366281123	-33.8319711956942	203.351407307145
H	-31.0877542522941	-32.8531302019386	203.067694531617
H	-30.0335539774933	-34.2104355718322	203.227676267799
O	-26.2663733673271	-39.2661245390802	204.747517206910
H	-25.5068111501035	-39.6188106978803	205.193948493838
H	-26.1922162693872	-38.2782626321436	204.669934127452
O	-27.7270291879377	-39.1992347887241	202.331464721096
H	-26.9738331416470	-39.5112261561240	202.942230941929
H	-28.4721755633441	-39.1541867389114	202.989824955093
O	-27.1920628656176	-37.1265830289358	199.545490624022
H	-26.5096639710603	-37.7976265249875	199.299201454892
H	-27.0863516593668	-36.3510665360432	198.935394715964
O	-26.7715519650315	-35.6925819484266	196.769593964345
H	-26.2450777709150	-36.5465967411663	196.754612533421
H	-27.6479681610520	-35.9276994250532	196.545302439852
O	-25.9181936186368	-33.9235995349074	198.772872027643
H	-26.2905465649640	-34.3817974023512	197.954600745912
H	-25.3247241914701	-33.1241577864628	198.491763033920
O	-28.1599891985197	-31.6604683511828	198.903602963278
H	-28.2511771745739	-30.8149041571290	199.537625216720
H	-28.9586746471560	-31.8351741646396	198.434747215878
O	-24.4414678262312	-31.8747796794088	197.872052478334
H	-23.5931255098889	-31.6539583179881	198.362782662761
H	-25.0019498544539	-31.0667031265847	198.028838221545
O	-26.1210586772148	-29.7517360095981	198.108976351012
H	-26.3538361572512	-29.1959981369474	198.967092889759
H	-26.8503567567162	-30.4266553180457	198.109164406726
O	-30.4334646647419	-31.3798375590043	202.085221397213
H	-29.6913067232047	-31.8826720088930	201.815228407867
H	-30.1118760117643	-30.7111110306056	202.675167038678
O	-25.2950915061205	-39.1754533791499	199.218309128961
H	-26.1101342216412	-39.7218519096205	199.322925087395
H	-25.0879774213352	-38.9309008200494	200.144421708783
H	-25.3255616244778	-34.8105514217628	201.103603615773

Section VIII. Extended Acknowledgement

We acknowledge support by U.S. Department of Energy Grant DE-FG02-05ER15646 (GWB), DE-SC0001423 (VSB), and computer resources from NERSC and Yale University. MZE was funded by a Computational Materials and Chemical Sciences (CMCSN) project at Brookhaven National Laboratory under contract DE-AC02-98CH10886 with the U.S. Department of Energy and supported by its Division of Chemical Sciences, Geosciences & Biosciences, Office of Basic Energy Sciences. Computer resources were provided by the High performance Computing facilities at Yale University. The authors acknowledge Dr. Marcos Villarreal, Dr. Sandra Luber, Dr. Ivan Rivalta, Dr Sivakumar Sekharan and Dr. Vanesa Galassi for valuable discussions.

REFERENCES

1. Umena, Y., Kawakami, K., Shen, J. R., and Kamiya, N. (2011) Crystal structure of oxygen-evolving photosystem II at a resolution of 1.9 angstrom, *Nature 473*, 55-U65.
2. D.A. Case, T. A. D., T.E. Cheatham, III, C.L. Simmerling, J. Wang, R.E. Duke, R. Luo, R.C. Walker, W. Zhang, K.M. Merz, B. Roberts, S. Hayik, A. Roitberg, G. Seabra, J. Swails, A.W. Goetz, I. Kolossváry, K.F. Wong, F. Paesani, J. Vanicek, R.M. Wolf, J. Liu, X. Wu, S.R. Brozell, T. Steinbrecher, H. Gohlke, Q. Cai, X. Ye, J. Wang, M.-J. Hsieh, G. Cui, D.R. Roe, D.H. Mathews, M.G. Seetin, R. Salomon-Ferrer, C. Sagui, V. Babin, T. Luchko, S. Gusarov, A. Kovalenko, and P.A. Kollman (2012) AMBER 12, University of California, San Francisco.
3. Phillips, J. C., Braun, R., Wang, W., Gumbart, J., Tajkhorshid, E., Villa, E., Chipot, C., Skeel, R. D., Kale, L., and Schulten, K. (2005) Scalable molecular dynamics with NAMD, *J Comput Chem 26*, 1781-1802.
4. Sproviero, E. M., Gascon, J. A., McEvoy, J. P., Brudvig, G. W., and Batista, V. S. (2008) Quantum mechanics/molecular mechanics study of the catalytic cycle of water splitting in photosystem II, *J Am Chem Soc 130*, 3428-3442.
5. Vreven, T., and Morokuma, K. (2000) The ONIOM (our own N-layered integrated molecular orbital plus molecular mechanics) method for the first singlet excited (S-1) state photoisomerization path of a retinal protonated Schiff base, *J Chem Phys 113*, 2969-2975.
6. Frisch, M. J., Trucks, G. W., Schlegel, H. B., Scuseria, G. E., Robb, M. A., Cheeseman, J. R., Scalmani, G., Barone, V., Mennucci, B., Petersson, G. A., Nakatsuji, H., Caricato, M., Li, X., Hratchian, H. P., Izmaylov, A. F., Bloino, J., Zheng, G., Sonnenberg, J. L., Hada, M., Ehara, M., Toyota, K., Fukuda, R., Hasegawa, J., Ishida, M., Nakajima, T., Honda, Y., Kitao, O., Nakai, H., Vreven, T., Montgomery, J. A., Jr., J. E. P., Ogliaro, F., Bearpark, M., Heyd, J. J., Brothers, E., Kudin, K. N., Staroverov, V. N., Kobayashi, R., Normand, J., Raghavachari, K., Rendell, A., Burant, J. C., Iyengar, S. S., Tomasi, J., Cossi, M., Rega, N., Millam, J. M., Klene, M., Knox, J. E., Cross, J. B., Bakken, V., Adamo, C., Jaramillo, J., Gomperts, R., Stratmann, R. E., Yazyev, O., Austin, A. J., Cammi, R., Pomelli, C., Ochterski, J. W., Martin, R. L., Morokuma, K., Zakrzewski, V. G., Voth, G. A., Salvador, P., Dannenberg, J. J., Dapprich, S., Daniels, A. D., Farkas, Ö., Foresman, J.

B., Ortiz, J. V., Cioslowski, J., and Fox, D. J. (2009) Gaussian 09, Revision A.1, *Gaussian 09*.
7. Becke, A. D. (1988) Density-functional exchange-energy approximation with correct asymptotic behavior, *Phys Rev A 38*, 3098-3100.
8. Becke, A. D. (1993) Density-functional thermochemistry. III. The role of exact exchange, *J. Chem. Phys. 98*, 5648-5652.
9. Hay, P. J., and Wadt, W. R. (1985) Abinitio Effective Core Potentials for Molecular Calculations - Potentials for the Transition-Metal Atoms Sc to Hg, *J Chem Phys 82*, 270-283.
10. Wadt, W. R., and Hay, P. J. (1985) Abinitio Effective Core Potentials for Molecular Calculations - Potentials for Main Group Elements Na to Bi, *J Chem Phys 82*, 284-298.
11. Hariharan, P. C., and Pople, J. A. (1973) Influence of Polarization Functions on Molecular-Orbital Hydrogenation Energies, *Theor Chim Acta 28*, 213-222.
12. Kirkpatrick, S., Gelatt, C. D., and Vecchi, M. P. (1983) Optimization by Simulated Annealing, *Science 220*, 671-680.
13. Ankudinov, A. L., Bouldin, C. E., Rehr, J. J., Sims, J., and Hung, H. (2002) Parallel calculation of electron multiple scattering using Lanczos algorithms, *Physical Review B 65*, 104107.
14. Newville, M. (2001) IFEFFIT: interactive XAFS analysis and FEFF fitting, *Journal of Synchrotron Radiation 8*, 322-324.
15. Grundmeier, A., and Dau, H. (2012) Structural models of the manganese complex of photosystem II and mechanistic implications, *Biochim Biophys Acta 1817*, 88-105.
16. Galstyan, A., Robertazzi, A., and Knapp, E. W. (2012) Oxygen-evolving Mn cluster in photosystem II: the protonation pattern and oxidation state in the high-resolution crystal structure, *J Am Chem Soc 134*, 7442-7449.
17. Luber, S., Rivalta, I., Umena, Y., Kawakami, K., Shen, J. R., Kamiya, N., Brudvig, G. W., and Batista, V. S. (2011) S1-state model of the O2-evolving complex of photosystem II, *Biochemistry 50*, 6308-6311.
18. Kurashige, Y., Chan, G. K., and Yanai, T. (2013) Entangled quantum electronic wavefunctions of the Mn4CaO5 cluster in photosystem II, *Nat Chem 5*, 660-666.